Inorganic Chemistry

Article

pubs.acs.org/IC

# Synthesis and Characterization of $Th_2N_2(NH)$ Isomorphous to $Th_2N_3$

G. W. Chinthaka Silva,*[,†,‡] Charles B. Yeamans,[§] Philppe F. Weck,[∥] John D. Hunn,[†] Gary S. Cerefice,[‡] Alfred P. Sattelberger,[⊥] and Ken R. Czerwinski[‡]

[†]Fuel Cycle and Isotopes Division, Oak Ridge National Laboratory, Oak Ridge, Tennessee 37831-6093, United States

[‡]Department of Chemistry, University of Nevada, Las Vegas, Box 454009, 4505 Maryland Parkway, Las Vegas, Nevada 89154, United States

[§]Chemical Sciences Division, Lawrence Livermore National Laboratory, 7000 East Avenue, L-550, Livermore, California 94551, United States

[∥]Sandia National Laboratories, P.O. Box 5800, MS 0779, Albuquerque, New Mexico 87185-0779, United States

[⊥]Energy Sciences and Engineering Directorate, Argonne National Laboratory, 9700 Cass Avenue, Argonne, Illinois 60439, United States

Supporting Information

**ABSTRACT:** Using a new, low-temperature, fluoride-based process, thorium nitride imide of the chemical formula $Th_2N_2(NH)$ was synthesized from thorium dioxide via an ammonium thorium fluoride intermediate. The resulting product phase was characterized by powder X-ray diffraction (XRD) analysis and was found to be crystallographically similar to $Th_2N_3$. Its unit cell was hexagonal with a space group of $P3\bar{m}1$ and lattice parameters of $a = b = 3.886(1)$ and $c = 6.185(2)$ Å. The presence of −NH in the nitride phase was verified by Fourier transform infrared spectroscopy (FTIR). Total energy calculations performed using all-electron scalar relativistic density functional theory (DFT) showed that the hydrogen atom in the $Th_2N_2(NH)$ prefers to bond with nitrogen atoms occupying 1a Wyckoff positions of the unit cell. Lattice fringe disruptions observed in nanoparticle areas of the nitride species by high-resolution transmission electron microscopic (HRTEM) images also displayed some evidence for the presence of −NH group. As $ThO_2$ was identified as an impurity, possible reaction mechanisms involving its formation are discussed.

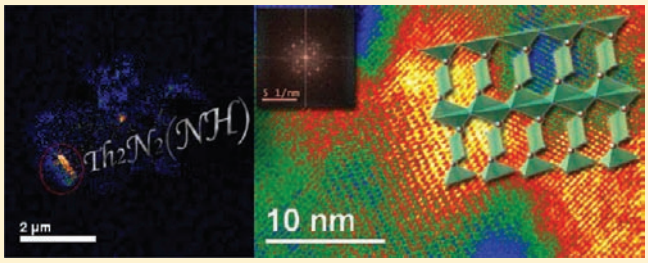


## 1. INTRODUCTION

Thorium nitride has a number of potential applications for nuclear systems, such as its incorporation into mixed actinide nitride fuels for breeder reactor concepts as well as the potential use in subcritical accelerator-driven systems. Thorium mononitride (ThN) is typically synthesized from thorium metal or oxide by first converting the metal to higher thorium nitrides, such as $Th_2N_3$[1,2] and $Th_3N_4$,[3−6] then thermally decomposing these species to the mononitride product. Stoichiometry of thorium nitrides is somewhat limited compared to multioxidation state actinides such as uranium and neptunium. However, literature has reported chemical compositions of thorium nitrides such as the controversial sesquinitride, $Th_2N_3$, where the oxidation number of thorium is nominally +4.5. Chiotti et al. reported the formation of $Th_2N_3$ when thorium metal is heated to 750 °C under $NH_3$.[1] Synthesis of the same compound was also reported by thermally decomposing thorium hydride at temperatures below 1500 °C under nitrogen or ammonia.[2] Previous identification of $Th_2N_3$ was later called into question due to its crystallographic structure resemblance to $Th_2N_2O$.[7] Benz et al.[8] also reported $Th_2N_3$ to be structurally equivalent to $Th_2N_2O$, which was synthesized by reacting ThN with $ThO_2$ at 1700 °C under a nitrogen atmosphere. Another study reported $Th_2N_3$ to be unstable at temperatures higher than 1500 °C under nitrogen or ammonia atmospheres.[2] Whereas there are only a few number of publications related to the chemistry of $Th_2N_3$ and $Th_2N_2O$, none has discussed the presence of thorium in an apparent oxidation state greater than +4 as in the case of $Th_2N_3$ .

The phase purity of the ThN depends on a number of factors such as heating atmosphere, temperature, and time.[3,6] If the temperature is not high enough, decomposition of $Th_3N_4$ may result in the formation of ThN with secondary chemical phases. At high temperatures, $Th_3N_4$ can be completely decomposed to ThN, but the literature also shows that secondary phases of $ThO_2$ and $Th_2N_2O$ readily form in addition to ThN. Formation of these secondary phases, especially $ThO_2$, has also been found in synthetic routes of higher thorium nitrides ($Th_xN_y$).[1] Formation of $ThO_2$ in $Th_3N_4$ even at room temperature has also been reported.[3] Minute quantities of $ThO_2$ present in thorium nitride systems can react with ThN to form $Th_2N_2O$, thus

Received: January 4, 2012
Published: February 23, 2012

   dx.doi.org/10.1021/ic300025b | Inorg. Chem. 2012, 51, 3332−3340

reducing the phase purity, even under inert atmospheric conditions.[3] Some of these issues have been investigated in previous kinematics[3,6] and thermodynamics[6] studies. However, not many microscopic studies have been conducted to explore the phase purity issues found in the thorium nitrides. Furthermore, the higher nitrides have not been sufficiently studied to support the process engineering necessary for viable plant-scale production of thorium mononitride.

In this current study, solid state reaction of different thorium fluorides with lithium amide ($LiNH_2$) under $NH_3$ was studied for the formation of thorium nitrides. Similar to the literature, the current study also reports formation of considerable secondary $ThO_2$ phases in higher thorium nitride/imides. Even though the experimental optimization to reduce the secondary phase formation is not discussed, microstructural and nanostructural characterization of the materials are presented as a basis for possible reaction mechanisms involved in oxide formation. Characterization of the samples was done using X-ray powder diffraction (XRD), Fourier transform infrared spectroscopy (FTIR), scanning electron microscopy (SEM), and transmission electron microscopy (TEM). Initial chemical phase identifications were performed with XRD and FTIR. Microscopy was used in further identifying and confirming the reaction sequence involved in the formation of the nitrides followed by thorium oxonitride and oxide. Density functional theory (DFT) calculations were used, along with the observed nanostructure of the product materials, to attempt to elucidate the crystal chemistry of the thorium nitride system. These results were employed in discussing the existence of $Th_2N_2(NH)$ in which the oxidation state of Th is compensated by a −NH group while preserving the crystallography of $Th_2N_3$ structure.

## 2. EXPERIMENTAL AND COMPUTATIONAL DETAILS

**2.1. Solid State Sample Synthesis.** Reactions involved with three thorium fluorides precursors ($(NH_4)_4ThF_8$, $ThF_4$, and ThNF) were examined. Single-phased $(NH_4)_4ThF_8$ was synthesized by reacting solid $ThO_2$ with solid $NH_4HF_2$. Ammonolysis of $(NH_4)_4ThF_8$ was performed utilizing the same experimental conditions used to synthesize the $ThF_4$ and ThNF.[9] Phase purity of each of these fluorides was confirmed with powder XRD analysis. To minimize oxygen contamination, samples were prepared using a platinum sheet or crucible, along with a zirconia sponge as an oxygen getter.[9,10] The samples were closed with another sheet of platinum to minimize the direct contact of any minute quantities of oxygen contaminants that could be generated from quartz at elevated temperatures. The $LiNH_2$ (95%, Alfa Aesar) was placed in an argon filled glovebox at all times to prevent moisture absorption. The $LiNH_2$ was analyzed by XRD and minor impurity levels of LiOH and $LiOH{\cdot}H_2O$ were found.

To synthesize the thorium nitrides, the above-mentioned thorium-based fluorides were admixed with $LiNH_2$ at either 1:1 or 1:4 molar ratio of thorium fluoride/$LiNH_2$. Some samples were made by grinding the reactants using a mortar and pestle for 5−10 min in air after transferring the $LiNH_2$ from the glovebox. The mixed sample was placed on an open or enveloped (platinum foil) inside a quartz tube. After purging the system[10] with an inert argon cover gas, the mixture was heated at 800 °C for 30 min under a flowing $NH_3$ gas. To minimize any further ingrowth of oxides following the synthesis, all of the characterizations were performed with freshly prepared samples. (***Note***: *$^{232}Th$ is a radioactive isotope and should be handled carefully with appropriate safety measures applied.*)

**2.2.1. Characterization Methods.** *X-ray Powder Diffraction Analysis.* X-ray powder diffraction patterns were obtained using a PANalytical X'Pert Pro MPD instrument with Cu−K$\alpha$ radiation filtered by Ni and using 40 mA current and 40 kV voltage. The Rietveld method was used to analyze each powder pattern using the XRD pattern fitting program GSAS.[11] The phase compositions used to evaluate the reaction kinetics of the oxidation of the thorium nitride product were determined by this method.

*2.2.2. Fourier Transform Infrared Spectroscopy Analysis.* Samples were subjected to FTIR measurements after confirming the chemical phases by XRD analysis. Thorium nitride samples were mixed with potassium bromide (0.2−1% $ThN_x$ by mass) and pressed into thin, transparent, 13-mm-diameter disks. These disks were placed inside sampling cards (PIKE technologies) and loaded into the FTIR instrument. The FTIR instrument used was a Varian 3100 FT-IR Excalibur series with a Smith's Detection Durasample-IR in-compartment diamond attenuated total reflectance (ATR). Samples were analyzed for up to 33 days to explore the reaction kinetics qualitatively using FTIR.

*2.2.3. Electron Microscopy.* Scanning electron microscopic imaging was performed using a JEOL scanning electron microscope model JSM-5610 equipped with secondary electron (SE) and backscattered electron (BE) detectors and an Oxford ISIS EDS (energy dispersive spectroscopy) system. The acceleration voltage used in SEM was 15 kV. Transmission electron microscopic characterization performed in this study was carried out using a TECNAI-G2-F30 transmission electron microscope with a 300 keV field emission gun. Bulk morphology was analyzed under the conventional bright field (BF) mode, and microstructures/nanostructures were characterized using the high resolution TEM (HRTEM) mode. All TEM images were recorded using a slow scan CCD camera attached to a Gatan GIF 2000 image filter. Electron energy-loss spectrometry (EELS) was also used to obtain elemental maps of the samples. All the TEM sample slices of about 50−75 nm thick were prepared by microtome cutting.

*2.2.4. Density Functional Theory Calculations.* First-principles all-electron scalar relativistic calculations of the total energies and optimized geometries were performed using the spin-polarized DFT as implemented in the DMol3 computer code.[12,13] The exchange correlation energy was calculated using the generalized gradient approximation (GGA) with the parametrization of Perdew and Wang (PW91).[14] Double numerical basis (DNP) sets including polarization functions on all atoms were used in the calculations. The DNP basis set corresponds to a double-$\zeta$ quality basis set with d-type polarization functions added to atoms heavier than hydrogen. The DNP basis set is comparable to split-valence 6-31G** Gaussian basis sets[15] with a better accuracy for a similar basis set size. 6d, 7s, 7p, and 5f polarization functions were included in the Th basis set. In the generation of the numerical basis sets, a global orbital cutoff of 5.9 Å was used. The energy tolerance in the self-consistent field calculations was set to $10^{-6}$ Hartree. Optimized geometries were obtained using the direct inversion in a subspace (DIIS) method with an energy convergence tolerance of $10^{-5}$ Hartree and a gradient convergence of $2 \times 10^{-3}$ Hartree/Å. The Monkhorst-Pack special *k*-point scheme[16] was used for structural optimization calculations with a $7 \times 7 \times 4$ mesh.

## 3. RESULTS

**3.1. XRD and FTIR Analysis.** Initial experiments conducted at low temperatures showed that the starting materials ($(NH_4)_4ThF_8$ and $ThF_4$) did not decompose below 800 °C to produce any nitrides. Therefore, the mixed samples of the thorium-based fluorides and $LiNH_2$ were heated under $NH_3(g)$ at temperatures ≥800 °C. By powder XRD analysis, the primary product phase was identified as $Th_2N_3$ or an isomorphous chemical phase. A number of different chemical species such as $ThF_xO_y$ and $ThF_4$ were also identified in the products at these experimental conditions, especially when the reactant phase contained $LiNH_2$ and $(NH_4)_4ThF_8$. When $ThF_4$ or ThNF reacted with $LiNH_2$, the nitride phase was formed with no unreacted $LiNH_2$. Samples produced from the 1:4 molar ratio of $ThF_4$ to $LiNH_2$ were also found to contain LiF as a secondary phase. The samples made by heating 1:1 molar ratio of $ThF_4$/or ThNF to $LiNH_2$ produced the nitride with a secondary $ThO_2$ phase. In previous work on the same experimental


dx.doi.org/10.1021/ic300025b | Inorg. Chem. 2012, 51, 3332−3340

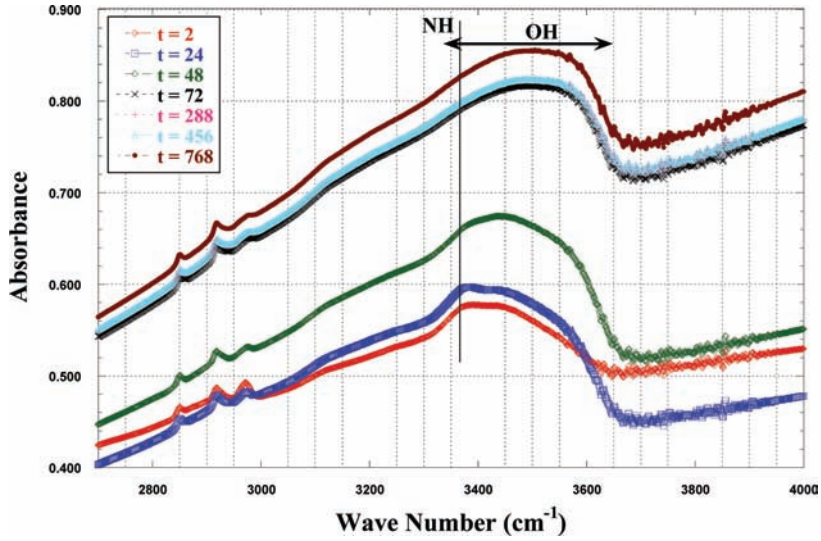


**Figure 1.** FTIR spectra of the sample synthesized by heating ThNF and $LiNH_2$ (1:1 molar ratio) mixed sample at 800 °C for 30 min under $NH_3$ as a function of time. Only the 2700 to 3900 $cm^{-1}$ region is shown for clarity of the −NH band disappearance. The time (t) given in the figure is in hours.

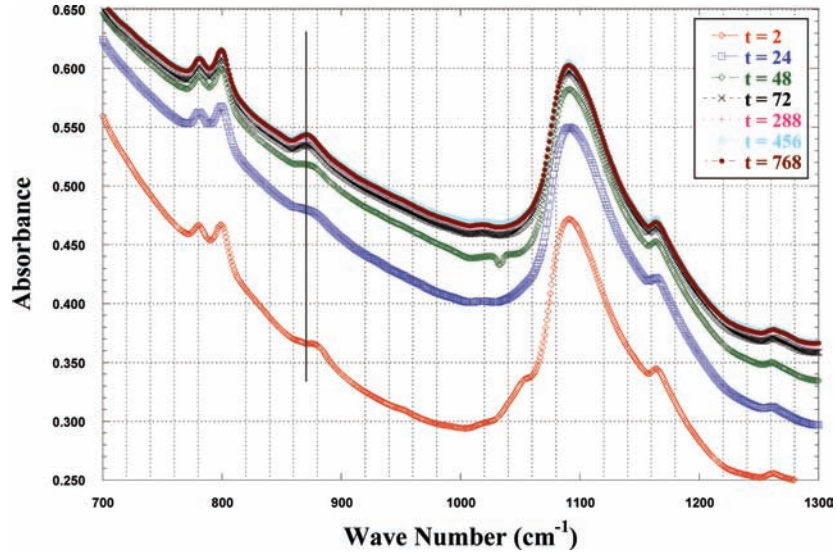


**Figure 2.** FTIR band shift of the −ThO (880 $cm^{-1}$) bonding in the sample in Figure 1 as a function of time. The time (t) given in the figure is in hours.

system, ThNF,[9] $UN_2$, $U_2N_3$, and 97 wt % UN[17] were able to be produced successfully. Based on these experiences, the considerable level of secondary oxide phase (≥15 wt %) observed in this system provides further evidence that the thorium nitride system is highly susceptible to oxygen contamination.

The FTIR study showed that the samples, which contained the chemical phase isomorphous to $Th_2N_3$, included a −NH band. This observation was prominent up to 3 days from the end of the sample preparation (48−72 h). Figure 1 displays an area of interest for −NH and −OH bands in one of the samples. The −OH stretching vibrations normally present in a wide range. For free OH and with intramolecular H bonds, sharp bands of −OH stretching vibrations will be present at 3610−3645 $cm^{-1}$ and 3450−3600 $cm^{-1}$, respectively. If intermolecular H bonds are present, broad −OH stretching at 3200−3550 $cm^{-1}$ will be observed.[18] Free −NH stretching vibrations are normally seen at 3300−3500 $cm^{-1}$, while H bonded NH will lie at 3070−3350 $cm^{-1}$.[18] In this sample (Figure 1), the usual broad band of −OH stretching vibration ranged from 3300 $cm^{-1}$ to 3650 $cm^{-1}$. This broad −OH stretching band was disrupted by the substantial −NH stretching band (highlighted by a vertical line), especially in the first 2 days. The −NH band could be differentiated from the overlapped broad −OH band in the spectra corresponding to the first 2 days and is slightly observable in the spectrum corresponding to the third day. Also, the broad −OH stretching vibration band shifted toward higher energy frequency than the usual range (3200−3550 $cm^{-1}$) probably due to intramolecular H bonding. This observation is prominent as the −NH band decreases. This suggests a time-dependent growth in the weak bonding character of −OH with −NH, corresponding to the oxidation of the NH group. The complete disappearance of the −NH band occurred within 72 h.

The presence of a −ThO band was also identified in the same sample[19,20] (Figure 2), probably due to the fast reaction of the −NH group with $O_2(g)$ or moisture. Furthermore, the


dx.doi.org/10.1021/ic300025b | Inorg. Chem. 2012, 51, 3332−3340

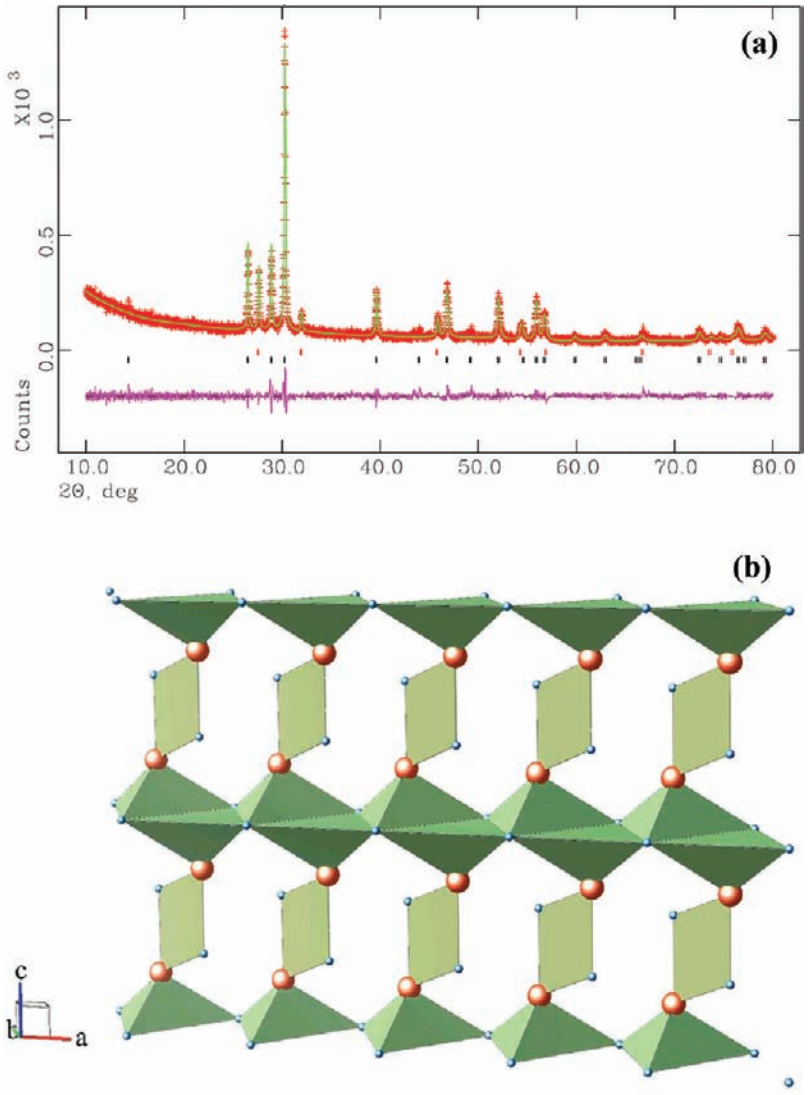


**Figure 3.** (a) XRD/Rietveld analysis of the $Th_2N_2(NH)$ sample synthesized by heating ThNF and $LiNH_2$ (1:1 molar ratio) mixed sample at 800 °C for 30 min under $NH_3$. The high background at the beginning is due to Kapton tape used to seal the sample. The red and green patterns are the experimental and calculated XRD patterns, respectively. The difference plot is given at the bottom of the figure. Upper (red) and bottom (black) tick marks are for $ThO_2$ and $Th_2N_2(NH)$ phases, respectively. $Th_2N_2(NH)$ phase weight percentage = 84.7 wt %. $ThO_2$ = 15.3 wt %. $\chi^2$ = 0.95. (b) A stack of $Th_2N_2(NH)$ unit cells with polyhedrons showing interatomic bonding.

**Table 1. Crystallographic Data of $Th_2N_2(NH)$ Isomorphous to $Th_2N_3$**

| space group | $a = b$ (Å) | $c$ (Å) | $\alpha = \beta$ | $\gamma$ | cell volume (Å$^3$) | density (gcm$^{-3}$) | cell formula units ($z$) |
|---|---|---|---|---|---|---|---|
| $P3\bar{m}1$ | 3.886(1) | 6.185(2) | 90 | 120 | 80.86(4) | 10.393 | 1 |
| atom | $x$ | $y$ | $z$ | frac | uiso (Å$^2$) | site sym | multiplicity |
| Th | 0.3333 | 0.6667 | 0.24168 | 1.0 | 0.0295 | 3M(100) | 2 |
| N(1) | 0 | 0 | 0 | 1.0 | 0.0297 | −3M(100) | 1 |
| N(2) | 0.3333 | 0.6667 | 0.64973 | 1.0 | 0.0298 | 3M(100) | 2 |

band shifted toward low wavenumbers (from 880 to 872 cm$^{-1}$) with time, indicating a lower energy associated with the bonding than that of the original compound at time. This is an indication of weakened hydrogen bonding due to a decrease in the −NH group concentration of the compound. These findings with respect to the chemical phases are presented in the Discussion section.

Figure 3a shows the analyzed powder XRD pattern of the $Th_2N_2(NH)$ sample produced by the ammonolysis of a 1:1 molar ratio of ThNF and $LiNH_2$ at 800 °C. The XRD pattern was analyzed assuming crystallography of $Th_2N_3$ since hydrogen atoms are poorly detected. The Rietveld-refined lattice parameters of the compound using a hexagonal $P3\bar{m}1$ unit cell are $a = b$ = 3.886(1) and c = 6.185(2) Å. Because these refined lattice parameters showed a good match to $a = b$ = 3.883 and c = 6.187 Å reported by Zachariasen et al.[7] (ICSD 76467) for $Th_2N_3$, the $Th_2N_2(NH)$ could be considered as isomorphous to the sesquinitride. A complete list of analyzed crystallographic information of the sample is given in Table 1.

In this unit cell (Figure 3b), the two Th atoms reside at (1/3 2/3 0.24) and (2/3 1/3 0.75) atomic coordinates. The eight N(1) lattice points in $Th_2N_2(NH)$ lie in the unit cell base


dx.doi.org/10.1021/ic300025b | Inorg. Chem. 2012, 51, 3332−3340

with atomic coordinates of (000), (001), (010), (011), (100), (101), (110), and (111). The two N(2) atoms lie at (1/3 2/3 0.65) and (2/3 1/3 0.35) positions. A stack of $Th_2N_2(NH)$ unit cells forming polyhedrons is shown in Figure 3b. Each of the two Th atoms bonds with three base N atoms at unit cell corners and the two N atoms inside the unit cell. Some selected interatomic bond distances of the crystal unit cell refined by XRD pattern are summarized in Table 2.

**Table 2. Selected Interatomic Distances for the Synthesized $Th_2N_2(NH)$ Sample**

| bond | distance (Å) | angle | angles (deg.) |
|---|---|---|---|
| Th−N(1) | 2.696 | N(1)−Th−N(1) | 112.117(6) |
| Th−N(2) | 2.342 | N(1)−Th−N(2) | 73.332(6) |
| | | Th−N(1)−Th | 106.668(6) |
| | | Th−N(2)−Th | 112.117(6) |

**3.2. DFT Calculations.** DFT calculations carried out for $Th_2N_2(NH)$ isormorphous to $Th_2N_3$ phase crystallizing in the $La_2O_3$-type hexagonal system with $P3\bar{m}1$ ($D3d$.3, IT 164) space group symmetry also supported the powder XRD results of $Th_2N_2(NH)$. Lattice parameters for the relaxed unit cell calculated from DFT are $a = b = 3.92$ Å and $c = 6.20$ Å ($c/a = 1.58$), i.e. less than 1% larger than observed experimentally. Even though FTIR analysis showed the thorium nitride sample to contain −NH group, the powder XRD cannot be used to confirm this finding due to hydrogen's low atomic number. To support the finding of the −NH group in the nitride sample, additional DFT calculations were performed. These calculations determined energetically favorable locations of the H atom within $Th_2N_2(NH)$ forming a N−H bond and assuming crystallography similar to that of $Th_2N_3$ unit cell. As summarized in Figure 4, results showed that the H atom preferentially forms a bond with N atoms occupying 1a Wyckoff positions (corner of the unit cell). Structures where the H atom is bound to N atoms in 2d positions (N atoms bridging Th atoms) have 0.33 to 0.52 eV/unit-cell higher total energies.

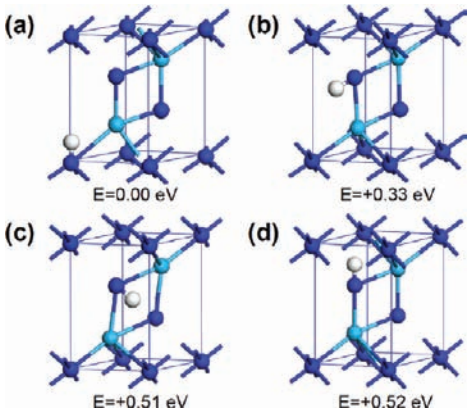


**Figure 4.** Possible crystallographic unit-cell geometries of $Th_2N_2(NH)$ calculated using all-electron scalar relativistic DFT. The total energy value per unit cell, E, for each structure (b)−(d) is given with respect to the most stable structure (a). Color legend: navy blue, N; cyan, Th; white, H.

**3.3. TEM and SEM Image Analysis.** The EELS elemental mappings of a reasonably separated cluster of the synthesized nitride sample are shown in Figure 5. Due to a thickness of the particles in the bulk region, only the sample edges and thin areas were successfully used in obtaining elemental maps, especially in the case of Th. Distribution of thorium was uniform throughout the grain edges. The N map shows a considerably large amount of nitrogen concentration distributed in two particle areas (bright red/yellow color) with respect to other regions. Therefore, these particle regions were further examined by HRTEM (Figure 6). A uniform distribution of oxygen could be observed throughout all the particles (Figure 5 O map), except on the particle area of high nitrogen concentration. For the observed particles these two observations infer oxygen-rich particle surfaces and a nitride chemical phase without a detectable oxygen contamination.

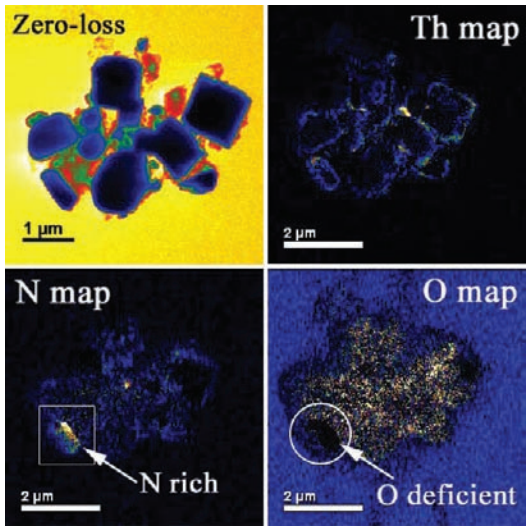


**Figure 5.** EELS elemental maps of $Th_2N_2(NH)$ sample.

HRTEM images were obtained on the thorium nitride particle with high nitrogen concentration (Figure 5 N map) while Figures 6 and 7 show different areas of this particle. Since lattice fringe spacing of HRTEM images correspond to crystal lattice planes as a function of $d$-spacing, the lattice fringe details were utilized to confirm the thorium nitride imide phase. If one nitrogen atom is associated to one hydrogen in the $Th_2N_2(NH)$ without altering the crystallography of $Th_2N_3$, then the $d$-spacing of crystallographic planes of $Th_2N_2(NH)$ should be close to that of $Th_2N_3$. This would lead to lattice fringe spacing in the HRTEM images corresponding to $d$-spacing of $P3\bar{m}1$ hexagonal $Th_2N_3$ crystallographic planes. Therefore, the crystallographic results obtained for the nitride sample in Section 3.1 are used in the $Th_2N_2(NH)$ analysis from this point onward.

Thus, Figure 6a and b indicate that the visible lattice fringes are from the (100) lattice plane reflections of $Th_2N_2(NH)$ aligned in the [010] beam direction. Most of the areas in Figure 6a do not contain clear lattice fringe details due to thickness contrast in the particle. However, the magnified area in Figure 6b consists of 2-directional lattice fringes of 3.88 Å fringe spacing corresponding to (100) reflections ($d$-spacing 3.8873 Å). The image also shows amorphous domains on a length scale of less than 2 nm. Furthermore, some of the lattice fringes (along AB) display disorientations in their atomic distributions. Corresponding experimental intensity profiles (Figure 6d and e) within one set of lattice fringes normal to the [100] direction indicate a disruption of atomic positioning along AB at point C. At this point, the atomic layer begins to continue along CB with


dx.doi.org/10.1021/ic300025b | Inorg. Chem. 2012, 51, 3332−3340

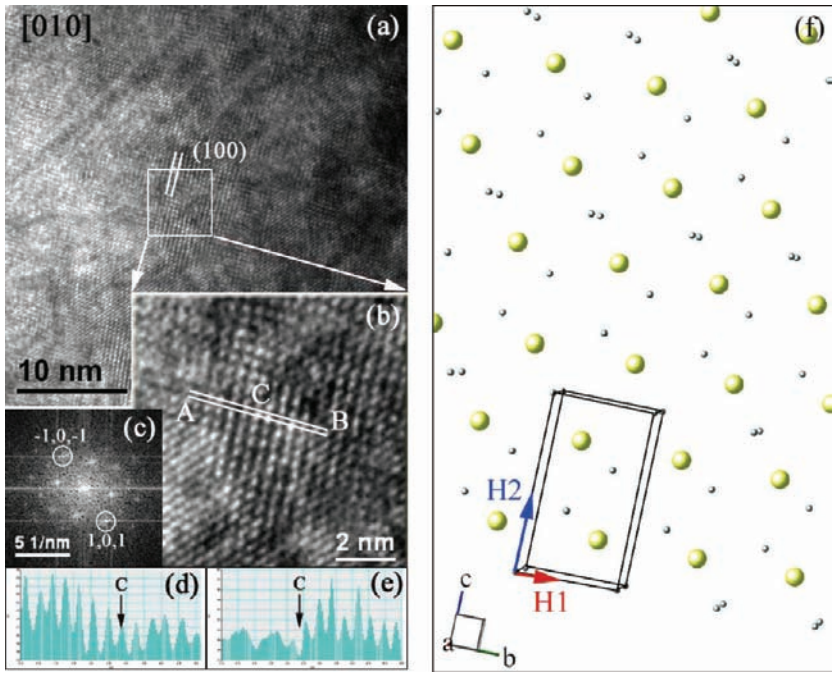


**Figure 6.** (a) HRTEM image of $Th_2N_2(NH)$ sample; (b) magnified image of the square area in (a); (c) FFT of (b); (d) and (e) are the experimental intensity profiles of the HRTEM image in (b) along the two lines denoted by AB. (f) A set of unit cell models representing (100) planes (rotated 10° clockwise). H1 and H2 represent examples of possible N−H bonding along *y* (or *x*) and *z* axis, respectively.

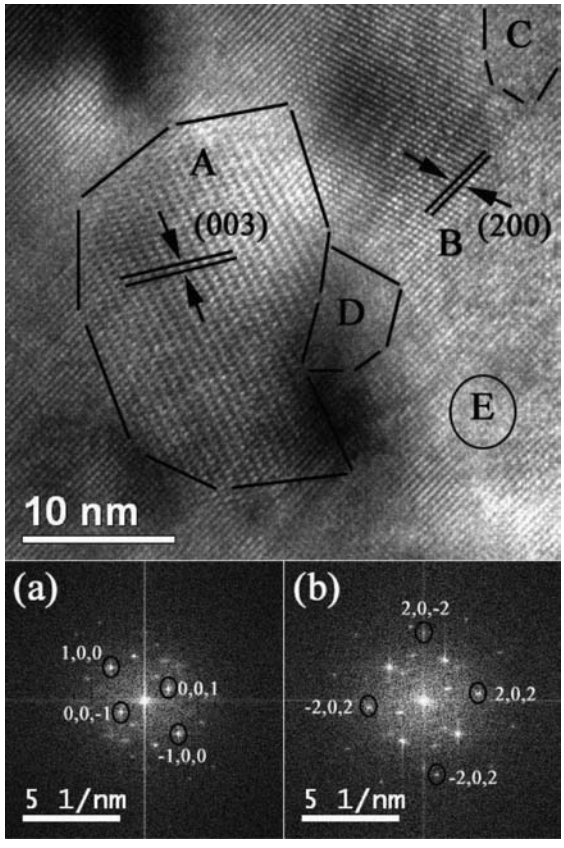


**Figure 7.** HRTEM (top) and the corresponding FFT micrographs of the synthesized $Th_2N_2(NH)$ sample (bottom). FFT in (a) and (b) correspond to the areas A and B in the HRTEM image, respectively.

a 0.1 nm shift normal to AB. This shift is close to twice the size of a hydrogen atom, based on the Bohr radius of 0.0529 nm. According to the DFT calculations, the H atom bonding to the N atom at corner of the unit cell is most energetically favorable. If the H atom binds at one of the unit cell corners, either along *a* or *b*-axis ("H1" in Figure 6f), then that set of unit cells would have symmetric hydrogen bonding leading to an aligned lattice fringe orientation due to (100) planes. If the H atoms are attached to N atoms in another set of unit cells along *c*-axis, as exemplified by "H2" in Figure 6f, then that set of unit cells could lead to a slight misalignment in the direction normal to the previous (100) planes. This is due to slight difference in the bonding characteristics in the unit cells because a = b ≠ c. The result could be the presence of slightly shifted lattice fringes in the compound's nanostructure as was observed (Figure 6b). This shift is attributed to the presence of an H atom and is twice its radius.

In Figure 7, a HRTEM image of another particle area is displayed together with fast Fourier transform (FFT) micrographs of two areas (A and B) of interest. Further characterization of this nanoscale particle area showed that lattice fringe details in these areas correspond to the nitride and the oxide of thorium, respectively. These FFT micrographs and the lattice fringe details indicate that area A with a lattice fringe spacing of 2.07 Å corresponds to the (003) reflections of $Th_2N_2(NH)$ (*d*-spacing 2.0623 Å) and area B with a lattice fringe spacing of 2.77 Å corresponds to the (200) reflections of $ThO_2$ (*d*-spacing 2.79885 Å) in the [010] beam direction. Basically, the nitride lattice fringes are surrounded by that of the oxide. The thorium oxide phase formation at nanoscale in such a manner is apparent due to prominent oxidation of the thorium nitride. Because no phase impurities were observed in the syntheses of thorium nitrides performed under conditions based on ThNF or $UN_x$, the above oxidation behavior implies thorium nitride/imide's high reactivity with oxygen in the experimental setup. This also suggests that thorium oxides are more thermodynamically stable than the corresponding nitrides. Some nanoscale amorphous patches were also observed, especially between the $Th_2N_2(NH)$ and $ThO_2$ lattice fringes


dx.doi.org/10.1021/ic300025b | *Inorg. Chem.* 2012, 51, 3332−3340

(Figure 8C). The presence of lattice fringes corresponding to the nitride phase surrounded by oxide phase at nanoscale indicates the nitride phase oxidation, while the amorphous areas identified infer an intermediate phase such as $Th_2N_2O$.

The secondary electron mode SEM images (Figure 8a and b) show the particle morphologies of the synthesized $Th_2N_2(NH)$

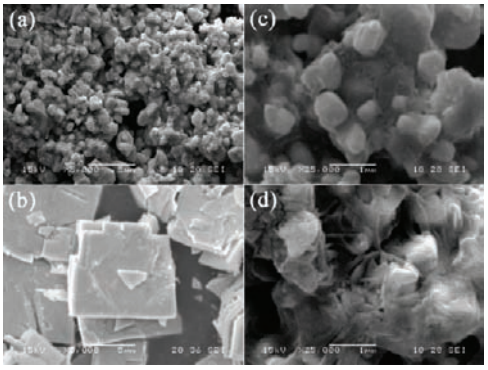


**Figure 8.** SEM images of nitride imides and oxides of thorium. (a) Synthesized $Th_2N_2(NH)$ sample at low resolution. (b) Reactant $ThO_2$. (c) $Th_2N_2(NH)$ surrounded by incompletely crystallized $ThO_2$ particles. (d) Plate-like $Th_2N_2(NH)$ particles.

sample and the reactant $ThO_2$, respectively. The incomplete plate-like character of the surface particles (Figure 8c) indicates that the needle-shaped $Th_2N_2(NH)$ particles (Figure 8d) are surrounded by the secondary $ThO_2$ particles. The presence of inner $Th_2N_2(NH)$ with outer $ThO_2$ microparticles signify that the $Th_2N_2(NH)$ was first formed during the ammonolysis of the fluorides. The amorphous like character in these particles could be attributed to agglomeration effects caused by grinding during SEM sample preparation for SEM specimen mounting.

**3.4. Reaction Sequence and Oxidation Behavior.** Different approaches were utilized in preparing the mixed reactants for the ammonolysis step to investigate any effects on the products. After each approach, the ammonolysis products were analyzed using XRD. Mixing and grinding $ThF_4$ with $LiNH_2$ formed $ThN_xF_y$ and $Li_3ThF_7$ (Figure 9). Reacting $ThF_4$

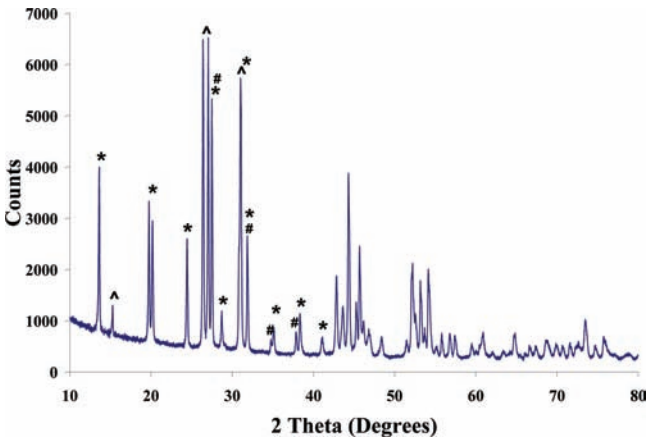


**Figure 9.** XRD powder pattern of the ammonolyzed $ThF_4$ mixed and ground with $LiNH_2$ (heated at 800 °C for 30 min). Peak positions of the product phases $Li_3ThF_7$ (ICSD 1726), ThNF (ICSD 35747), and $ThO_2$ (ICSD 61586) are denoted by *, ∧, and #, respectively.

with $LiNH_2$ by gentle admixing with a spatula produced the expected $Th_2N_2(NH)$. The results of these two experiments

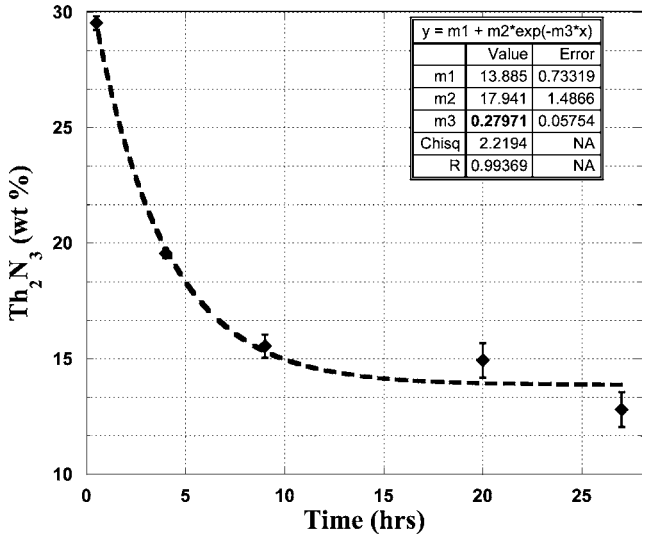


**Figure 10.** Reaction kinetics of $Th_2N_2(NH)$ with $O_2$ or moisture in air.

inferred the purity of the $LiNH_2$ was preserved for the sample preparation when transferring the reactants from the glovebox into the reaction setup. Grinding changed $LiNH_2$ into LiOH because of its high reactivity with air moisture.

The oxidation behavior of the thorium nitride imide synthesized in this study was also explored. Oxidation kinetics of $Th_2N_2(NH)$ was determined under ambient conditions. This study showed that the nitride sample has high reactivity toward air or moisture, even at room temperature (Figure 10). The nitride/imide phase rapidly oxidized, reaching a minimum concentration at 10 h after steady-state was achieved. An XRD pattern obtained after 47 h did not produce sufficient peak intensities for accurate phase quantity analysis of the nitride phase. Diminished intensity of the −NH band in the FTIR spectrum after 48 h spectrum (Figure 1) also confirmed this observation. Given these experimental details, the results acquired in this study on oxidation of the $Th_2N_2(NH)$ phase corresponded to a pseudo-first-order reaction with a $7.8 \times 10^{-5}$ $s^{-1}$ rate constant from the data up to 27 h.

## 4. DISCUSSION

Heating $(NH_4)_4ThF_8$ or $ThF_4$ under $NH_3(g)$ up to 1100 °C produces ThNF.[9] This reaction route was modified to produce thorium nitride (imide) by adding $LiNH_2$ into the reactant fluorides. Powder XRD studies indicated thorium nitride formation with a crystal structure similar to $Th_2N_3$ in a $La_2O_3$-type hexagonal unit cell with $P3\bar{m}1$ space group symmetry. The FTIR studies showed the presence of an −NH group suggesting a $Th_2N_2(NH)$ chemical formula for the nitride from the synthesis. Even though XRD alone was unable to detect the presence of the −NH, DFT calculations on a slightly modified $Th_2N_3$ type unit cell containing the hydrogen atom provided further insight into the stability of the $Th_2N_2(NH)$ structure and the hydrogen's energetically favorable location within the unit cell. These calculations supported the formation of −NH bonding in the compound without altering the crystal symmetry of the corresponding sesquinitride of thorium. These results confirmed the $Th_2N_2(NH)$ to have crystallography isomorphic to that of the $Th_2N_3$.

The EELS elemental mapping also confirmed the formation of a nitride species separated from the oxide or the oxonitride. Levels of nanoscale disruptions found in the nanostructure of


dx.doi.org/10.1021/ic300025b | Inorg. Chem. 2012, 51, 3332−3340

the nitrogen rich sample areas in HRTEM images were compatible to the bonding characteristics of the H atom with N atoms at the corners of the nitride unit cell predicted by DFT calculations. Formation of terminal $ThO_2$ due to thorium nitride imide oxidation was identified from its nanostructure details using HRTEM imaging. Also, amorphous patches in some of the particle areas between the imide and oxide domains further verified the time-dependent formation of another intermediate chemical phase, possibly $Th_2N_2O$, which completely transformed into the terminal high stable $ThO_2$. As pointed out by SEM analysis, the $Th_2N_2(NH)$ microparticles were surrounded by these secondary $ThO_2$ particles. The presence of inner $Th_2N_2(NH)$ plus the outer $ThO_2$ microparticles indicated that the $Th_2N_2(NH)$ was first formed during the ammonolysis of the fluorides. Also, fast reaction kinetics was observed for $Th_2N_2(NH)$ oxidation at ambient conditions with a pseudo-first-order rate constant of $7.8 \times 10^{-5}$ $s^{-1}$.

These details suggested the high susceptibility of the thorium nitride imide to $O_2$ or moisture in air. Thus, the majority of the oxide phase was speculated to be formed after the nitride imide was synthesized due to further oxidation of the nitride phase both under ambient and experimental conditions. Although discussing the optimization of the experimental conditions to synthesize phase pure thorium nitride is beyond the scope of this paper, these observations further verified the difficulty of making single-phased thorium nitrides as indicated in the literature has.

Because ThNF was the terminal product in the ammonolysis step of thorium-based fluorides, it can be assumed that ThNF was first formed, and it reacted with $LiNH_2$ to form the nitride (R1). When $(NH_4)_4ThF_8$ was used in the reactant phase, $ThF_xO_y$ species were identified. This observation implies that the nitride phase was produced by reaction R1. Intermediate phases of $(NH_4)_4ThF_8$ decomposition are the probable cause of $ThF_xO_y$ secondary chemical phases. Additional studies revealed one other reaction R2 that could increase the level of $ThO_2$ if $ThF_4$ was used in the reactant instead of ThNF. As seen with FTIR, the formed $Th_2N_2(NH)$ is unstable because of the high sensitivity of the −NH group to moisture, as in the case of $LiNH_2$. This could form the thorium oxonitride ($Th_2N_2O$) phase (R3). The HRTEM images also showed the presence of amorphous areas between the lattice fringes of nitride and oxide phases at nanoscale inferring intermediate $Th_2N_2O$ phase formation.

$$2ThNF + 2LiNH_2 \rightarrow Th_2N_2(NH) + 2LiF + NH_3 \quad (R1)$$

$$2ThF_4 + 4LiOH \rightarrow Li_3ThF_7 + LiF + ThO_2 + 2H_2O \quad (R2)$$

$$Th_2N_2(NH) + H_2O \rightarrow Th_2N_2O + NH_3 \quad (R3)$$

$$Th_2N_2O + 3H_2O \rightarrow 2ThO_2 + 2NH_3 \quad (R4)$$

Because $Th_2N_2O$ and $Th_2N_3/Th_2N_2(NH)$ have similar crystallography, it was difficult to differentiate these two compounds using powder XRD. Nevertheless, disappearance of the H-bonding characteristics with the formation of −ThO with time supports the proposition of $Th_2N_2O$ formation (R3). With time, $Th_2N_2O$ can easily react with $O_2$ in air or moisture producing $ThO_2$. Complete transformation of the nitride into $ThO_2$ within 48−72 h confirmed these observations.

## 5. CONCLUSIONS

Addition of $LiNH_2$ into a thorium fluoride reaction medium was studied. Initial characterization of the synthesized nitride samples demonstrated a chemical crystallography similar to that of $Th_2N_3$. Even though the crystallography of this nitride is similar to the oxonitride ($Th_2N_2O$), formation of the nitride microparticles separated from the oxide or oxonitrides were confirmed by EELS mapping and HRTEM imaging. FTIR studies revealed the presence of an −NH group in the nitride, proposing a chemical composition of $Th_2N_2(NH)$ for the nitrogen containing thorium phase in the samples. Comparison of experimental results and DFT calculations of the $Th_2N_3$ and $Th_2N_2(NH)$ showed that a crystal structure of $Th_2N_2(NH)$ isomorphous to $Th_2N_3$ is possible, while in the most stable configuration, the H atom will reside close to N atoms at corners of the unit cell. Because single-phased ThNF, $UN_2$, $U_2N_3$, and considerably high phase purity UN were synthesized using a similar experimental setup and only up to 90 wt % $Th_2N_2(NH)$ was made, it can be concluded that thorium system is more susceptible to oxygen contamination compared to uranium system. The oxidation kinetics also confirmed this finding.

## ■ ASSOCIATED CONTENT

### Supporting Information

The crystallographic information file (CIF) of thorium nitride imide. This material is available free of charge via the Internet at http://pubs.acs.org.

## ■ AUTHOR INFORMATION

### Corresponding Author

*E-mail silvagw@ornl.gov. Tel (865)574-6264. Fax (865)574-4186.

### Notes

The authors declare no competing financial interest.

## ■ ACKNOWLEDGMENTS

The research work performed at the University of Nevada, Las Vegas (UNLV) under the UNLV Transmutation Research Program, was funded by the U.S. Department of Energy (Grant DE-FG07-01AL67358). Work at Oak Ridge National Laboratory was sponsored by the U.S. Department of Energy Office of Nuclear Energy. Sandia National Laboratories is a multiprogram laboratory operated by Sandia Corporation, a wholly owned subsidiary of Lockheed Martin Company, for the United States Department of Energy's National Nuclear Security Administration under Contract DE-AC04-94AL85000. The authorsthank Dr. Anthony Hechanova for administrating the UNLV Transmutation Research Program, and Tom O'Dou and Trevor Low for laboratory management and radiation safety support for this work.

## ■ REFERENCES

(1) Chiotti, P. *J. Am. Ceram. Soc.* **1952**, *35*, 123.
(2) Olson, W. M.; Mulford, R. N. R. *J. Phys. Chem.* **1965**, *69*, 1223.
(3) Uno, M.; Katsura, M.; Miyake, M. *J. Less-Common Metals* **1986**, *121*, 615.
(4) Benz, R.; Hoffma, C. G.; Rupert, G. N. *J. Am. Chem. Soc.* **1967**, *89*, 191.
(5) Aronson, S.; Cisney, E.; Gingerich, K. A. *J. Am. Ceram. Soc.* **1967**, *50*, 248.
(6) Uno, M.; Katsura, M.; Miyake, M. *Inorg. Chim. Acta* **1987**, *140*, 123.

(7) Zachariasen, W. H. *Acta Crystallogr.* **1949**, *2*, 388.
(8) Benz, R.; Zacharisen, W. H. *Acta Crystallogr.* **1966**, *21*, 838.
(9) Silva, G. W. C.; Yeamans, C. B.; Cerefice, G. S.; Sattelberger, A. P.; Czerwinski, K. R. *Inorg. Chem.* **2009**, *48*, 5736.
(10) Silva, G. W. C.; Yeamans, C. B.; Ma, L.; Cerefice, G. S.; Czerwinski, K. R.; Sattelberger, A. P. *Chem. Mater.* **2008**, *20*, 3084.
(11) Larson, A. C.; Von Dreele, R. B. *General Structure Analysis System (GSAS)*; Los Alamos National Laboratory Report LAUR, 2004; pp 86−748.
(12) Delley, B. *J. Chem. Phys.* **1990**, *92*, 508−517.
(13) Delley, B. *J. Chem. Phys.* **2000**, *113*, 7756−7764.
(14) Wang, Y.; P. P., J. *Phys. Rev. B* **1992**, *45*, 13244−13249.
(15) Hehre, W. J.; L. R., Schleyer, P. R.; Pople, J. A. *Ab Initio Molecular Orbital Theory*; Wiley: New York, 1986.
(16) Monkhorst, H. J.; D. P., J. *Phys. Rev. B* **1976**, *13*, 5188−5192.
(17) Silva, G. W. C.; Yeamans, C. B.; Sattelberger, A. P.; Hartmann, T.; Cerefice, G. S.; Czerwinski, K. R. *Inorg. Chem.* **2009**, *48*, 10635−10642.
(18) http://infrared.als.lbl.gov/content/web-links/60-ir-band-positions.
(19) Green, D. W.; Reedy, G. T. *J. Mol. Spectrosc.* **1979**, *74*, 423.
(20) Gabelnick, S. D.; Reedy, G. T.; Chasanov, M. G. *J. Chem. Phys.* **1974**, *60*, 1167−1171.